Operational Retrieval of Atmospheric Temperature, Moisture, and Ozone from MODIS Infrared Radiances

SUZANNE W. SEEMANN AND JUN LI

Cooperative Institute for Meteorological Satellite Studies, University of Wisconsin—Madison, Madison, Wisconsin

W. PAUL MENZEL

Office of Research and Applications, NOAA/NESDIS, Madison, Wisconsin

LIAM E. GUMLEY

Cooperative Institute for Meteorological Satellite Studies, University of Wisconsin—Madison, Madison, Wisconsin

(Manuscript received 14 June 2002, in final form 31 January 2003)

ABSTRACT

The algorithm for operational retrieval of atmospheric temperature and moisture distribution, total column ozone, and surface skin temperature from the Moderate Resolution Imaging Spectroradiometer (MODIS) longwave infrared radiances is presented. The retrieval algorithm uses clear-sky radiances measured by MODIS over land and ocean for both day and night. The algorithm employs a statistical retrieval with an option for a subsequent nonlinear physical retrieval. The synthetic regression coefficients for the statistical retrieval are derived using a fast radiative transfer model with atmospheric characteristics taken from a dataset of global radiosondes of atmospheric temperature, moisture, and ozone profiles. Evaluation of retrieved total precipitable water vapor (TPW) is performed by a comparison with retrievals from the Geostationary Operational Environmental Satellite (GOES) sounder, radiosonde observations, and data from ground-based instrumentation at the Atmospheric Radiation Measurement (ARM) Program Cloud and Radiation Test Bed (CART) in Oklahoma. Comparisons over one and one-half years show that the operational regression-based MODIS TPW agrees with the microwave radiometer (MWR) TPW at the ARM CART site in Oklahoma with an rmse of 4.1 mm. For moist cases, the physical retrieval improves the retrieval performance. For dry atmospheres (TPW less than 17 mm), both physical and regression-based retrievals from MODIS radiances tend to overestimate the moisture by 3.7 mm on average. Global maps of MODIS atmospheric-retrieved products are compared with the Special Sensor Microwave Imager (SSM/I) moisture and Total Ozone Mapping Spectrometer (TOMS) ozone products. MODIS retrievals of temperature, moisture, and ozone are in general agreement with the gradients and distributions from the other satellites, and MODIS depicts more detailed structure with its improved spatial resolution.

1. Introduction

The development of global climate and weather models requires accurate monitoring of atmospheric temperature and moisture, as well as trace gases and aerosols. Until recently, continuous monitoring of changes in these parameters on a global scale has been difficult. The Moderate Resolution Imaging Spectroradiometer (MODIS) offers a new opportunity to improve global monitoring of temperature, moisture, and ozone distributions and changes therein. MODIS was launched onboard the National Aeronautics and Space Administration (NASA) Earth Observing System (EOS) *Terra* and *Aqua* platforms on 18 December 1999 and 4 May 2002, respectively. The instrument is a scanning spectroradiometer with 36 visible (VIS), near-infrared (NIR), and infrared (IR) spectral bands between 0.645 and 14.235 μm (King et al. 1992). For reference, Table 1 lists the MODIS infrared spectral bands. Figure 1 shows the spectral responses of the MODIS infrared bands relative to an atmospheric emission spectrum computed by a line-by-line (LBL) radiative transfer model (RTM) for the *U.S. Standard Atmosphere, 1976.*

The wide spectral range, high spatial resolution, and near-daily global coverage of MODIS enable it to observe the earth's atmosphere and continuously monitor changes. MODIS retrievals of atmospheric water vapor and temperature distributions are intended to advance understanding of the role played by energy and water cycle processes in determining the earth's weather and

Corresponding author address: Suzanne Wetzel Seemann, CIMSS/SSEC, University of Wisconsin—Madison, Madison, WI 53706.
E-mail: swetzel@ssec.wisc.edu

TABLE 1. MODIS infrared band specifications: bandwidth (μm), spectral radiance values (W m^{-2} sr^{-1} μm^{-1}), reference temperature (K), and the noise-equivalent temperature difference NEΔT (K). Information was obtained online at http://modis.gsfc.nasa.gov/about/specs.html.

Primary use	Band	Bandwidth (μm)	Spectral radiance (and reference temperature) (K)	Required NEΔT (K)
Surface temperature	20	3.660–3.840	0.45 (300)	0.05
	21	3.929–3.989	2.38 (335)	2.00
	22	3.929–3.989	0.67 (300)	0.07
	23	4.020–4.080	0.79 (300)	0.07
Temperature profile	24	4.433–4.498	0.17 (250)	0.25
	25	4.482–4.549	0.59 (275)	0.25
Cirrus clouds/water vapor	27	6.535–6.895	1.16 (240)	0.25
	28	7.175–7.475	2.18 (250)	0.25
	29	8.400–8.700	9.58 (300)	0.05
Ozone	30	9.580–9.880	3.69 (250)	0.25
Surface temperature	31	10.780–11.280	9.55 (300)	0.05
	32	11.770–12.270	8.94 (300)	0.05
Temperature profile	33	13.185–13.485	4.52 (260)	0.25
	34	13.485–13.785	3.76 (250)	0.25
	35	13.785–14.085	3.11 (240)	0.25
	36	14.085–14.385	2.08 (220)	0.35

climate. MODIS temperature and moisture products can be used together with other satellite measurements in numerical weather prediction models in the regions where conventional meteorological observations are sparse. Determination and validation of various land, ocean, and atmospheric products, such as sea surface temperature, land surface temperature, and ocean aerosol properties, require temperature and moisture profiles, as well as total ozone at MODIS spatial resolution as ancillary input.

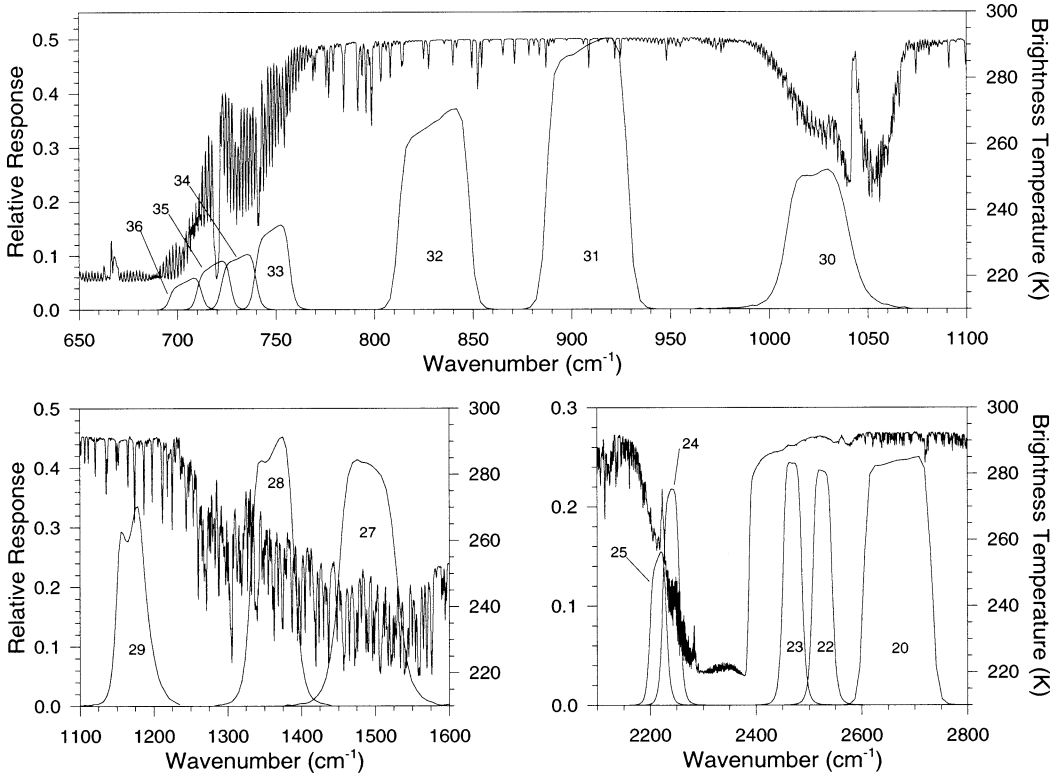

FIG. 1. MODIS infrared spectral response functions (numbered by MODIS band) and nadir-viewing brightness temperature spectrum of the *U.S. Standard Atmosphere, 1976* computed by LBL RTM.

The advantage of MODIS for retrieving the distribution of atmospheric temperature and moisture is its combination of shortwave and longwave infrared spectral bands (3–14.5 μm) that are useful for sounding and its high spatial resolution that is suitable for imaging (1 km at nadir). The increased spatial resolution of MODIS measurements delineates horizontal gradients of moisture, temperature, and atmospheric total ozone better than companion instruments, such as the Geostationary Operational Environmental Satellite (GOES) sounder [10-km resolution for single field-of-view (FOV) retrievals], Advanced Microwave Sounding Unit (AMSU; 45-km resolution)-A, High-Resolution Infrared Radiation Sounder (HIRS; 19-km resolution), and Atmospheric Infrared Sounder (AIRS; 15-km resolution). However, the MODIS broadband spectral resolution provides only modest information content regarding vertical profiles. True sounder radiances with higher spectral resolution, such as AIRS and the Cross-Track Infrared Sounder (CrIS) of the National Polar-Orbiting Environmental Satellite System (NPOESS), contain more information about the atmospheric vertical distribution of temperature and moisture. Because of the limited spectral resolution of MODIS, the strength of its retrieved products lies in the resolution of horizontal gradients and the distribution of retrieved quantities in integrated vertical layers (as opposed to vertical profiles).

This paper details the operational MODIS algorithm for retrieving atmospheric temperature and moisture distributions, total column ozone burden, and integrated total precipitable water vapor. This algorithm is also referred to as the MOD07 algorithm. The retrievals are performed using clear-sky radiances measured by MODIS within a 5 $\times$ 5 field of view (approximately 5-km resolution) over land and ocean for both day and night. The MOD07 algorithm is operational at the Goddard Distributed Active Archive Center (GDAAC) processing system. A version of the algorithm is also available for local processing of MODIS data, such as that received from a direct broadcast antenna, with the International MODIS/AIRS Processing Package (IMAPP) developed at the Space Science and Engineering Center (SSEC) at the University of Wisconsin—Madison (information available online at http://cimss.ssec.wisc.edu/~gumley/IMAPP/IMAPP.html).

Section 2 describes the retrieval algorithm. Section 3 outlines the implementation of the retrieval, including cloud detection, radiance bias adjustments, the training dataset, and a technique for eliminating the IR shortwave surface emissivity uncertainty in the retrievals. Section 4 presents some evaluation of MODIS atmospheric products. A discussion of retrieval errors and other issues affecting the atmospheric retrievals is in section 5. Section 6 offers some conclusions and plans for future work.

2. Algorithm development

The MODIS atmospheric temperature, moisture, and ozone retrieval algorithm is a statistical synthetic regression with the option for a subsequent nonlinear physical retrieval. The retrieval procedure involves linearization of the radiative transfer model and inversion of radiance measurements. To derive the statistical synthetic regression coefficients, MODIS infrared band radiances are calculated from radiosonde observations of the atmospheric state, generating an ensemble of computed radiances with associated observed atmospheric profiles. The radiative transfer calculation of the MODIS spectral band radiances is performed using a transmittance model called Pressure-Layer Fast Algorithm for Atmospheric Transmittances (PFAAST) (Hannon et al. 1996; Eyre and Woolf 1988); this model has 101 pressure-level vertical coordinates from 0.05 to 1100 hPa. The fast transmittance model uses LBL RTM calculations obtained with the LBL RTM, version 6.01, program and the high-resolution transmission molecular absorption spectroscopic database HITRAN 2000 (Rothman et al. 1998). The calculations take into account the satellite zenith angle, absorption by well-mixed gases [including nitrogen, oxygen, and carbon dioxide (CO_2)], water vapor (including the water vapor continuum), and ozone. The retrieval algorithms are developed in this section.

a. Radiative transfer model and its linearization

If scattering by the atmosphere is neglected, the true clear radiance exiting the earth–atmosphere system for a given MODIS IR band with center wavenumber υ is approximated by

$$R_\upsilon = \varepsilon B_s \tau_s - \int_0^{p_s} B \, d\tau(0, p) + (1 - \varepsilon) \int_0^{p_s} B \, d\tau^* + R', \quad (1)$$

where R_υ is the spectral radiance with wavenumber υ, $\tau(0, p)$ is the total transmittance from the top of the atmosphere to the atmospheric pressure p, ε is the surface emissivity, B is the Planck radiance, which is a function of pressure p, subscript s denotes surface, $\tau^* = \tau_s^2/\tau$ is the downwelling transmittance, and R' represents the contribution of reflected solar radiation in the infrared region. The reflected infrared solar radiation is considered negligible for bands with wavelengths longer than 4.0 μm during the day.

If the MODIS-observed radiance R_υ^m (m denotes MODIS) of each band is known, then R_υ^m can be considered a nonlinear function of the atmospheric properties, including the temperature profile, water vapor mixing ratio profile, ozone mixing ratio profile, surface skin temperature, and surface emissivity. That is, $R_\upsilon^m = R_\upsilon(T, q, O_3, T_s, \varepsilon, \ldots\ldots) + \sigma_\upsilon$, where σ_υ is the instrument noise and other sources of error, or, in general,

$$\mathbf{R}^m = \mathbf{R}(\mathbf{X}) + \boldsymbol{\sigma}, \tag{2}$$

where the vector $\mathbf{X}$ contains L (levels of atmosphere) atmospheric temperatures (T), L atmospheric water vapor mixing ratios (q), L atmospheric ozone mixing ratios (O_3) (the water vapor or ozone is expressed as the logarithm of the mixing ratio in practical applications), one surface skin temperature, two infrared surface emissivities at 909 and 2500 wavenumbers, and $\mathbf{R}^m$ contains N (number of MODIS spectral bands used) observed radiances.

To linearize Eq. (1), the first-order variations of the Planck and spectral radiances $\delta B = (\partial B/\partial T)\delta T$ and $\delta R = (\partial R/\partial Tb)\delta \mathrm{Tb}$ are used, where Tb is the brightness temperature. The linearized form of Eq. (1) is

$$\delta \mathrm{Tb}_\upsilon = W_{T_s}\delta T_s + \int_0^{p_s} W_T \delta T\, dp + \int_0^{p_s} W_q \delta \ln q\, dp + \int_0^{p_s} W_{o_3}\delta \ln O_3\, dp, \tag{3}$$

where Tb_υ is the brightness temperature for the MODIS IR spectral band with center wavenumber υ; W_T, W_q, and W_{o_3} are the weighting functions (sensitivity functions) of the atmospheric temperature profile, water vapor mixing ratio profile, and ozone mixing ratio profile, respectively. The weighting functions can be calculated efficiently from a given atmospheric state (Li 1994; Li et al. 2000):

$$W_{T_s} = \beta_s \tau_s \varepsilon, \tag{4a}$$

$$W_T(p) = -\beta\frac{\partial \tau}{\partial p} + \beta(1-\varepsilon)\frac{\partial \tau^*}{\partial p}, \tag{4b}$$

$$W_q(p) = \left[(T_s - T_a)\varepsilon\tau_s\beta_s - 2(1-\varepsilon)\int_0^{p_s}\beta\tau^*\frac{\partial T}{\partial p}\,dp\right]\frac{\partial \ln\tau_q}{\partial p} + \left\{\int_p^{p_s}\beta[\tau + (1-\varepsilon)\tau^*]\frac{\partial T}{\partial p}\,dp\right\}\frac{\partial \ln\tau_q}{\partial p}, \tag{4c}$$

$$W_{o_3}(p) = \left[(T_s - T_a)\varepsilon\tau_s\beta_s - 2(1-\varepsilon)\int_0^{p_s}\beta\tau^*\frac{\partial T}{\partial p}\,dp\right]\frac{\partial \ln\tau_{o_3}}{\partial p} + \left\{\int_p^{p_s}\beta[\tau + (1-\varepsilon)\tau^*]\frac{\partial T}{\partial p}\,dp\right\}\frac{\partial \ln\tau_{o_3}}{\partial p}, \tag{4d}$$

where $\beta(p) = \partial B/\partial T/\partial R/\partial Tb$ and τ_q and τ_{o_3} are the water vapor and ozone component transmittance functions, respectively. Figure 2a shows the temperature-weighting functions for the MODIS IR bands 20–25 and bands 27–36 calculated for a *U.S. Standard Atmosphere, 1976.* Bands 27 and 28 are water vapor absorption bands. However, these bands also provide information about the atmospheric temperature if there is enough moisture in the atmosphere, and provided that the water vapor profile is known or estimated accurately. Bands 33–36 are CO_2 absorption bands that also provide atmospheric temperature information; they can be used to infer the cloud properties with a known atmospheric temperature profile (Frey et al. 1999; Li et al. 2001). The moisture-weighting functions in Fig. 2b show that bands 27 and 28 provide information about the distribution of moisture in the troposphere, and that the window bands 29, 31, and 32 also provide some moisture information due to weak water vapor absorption. The weighting functions in Figures 2a and 2b were computed without any contrast between surface air temperature and surface skin temperature. Under these conditions, MODIS has limited skill in retrieving boundary layer temperature and moisture information. However, if contrast exists between the surface air temperature and surface skin temperature, information about the boundary layer moisture structure can be retrieved with more success. A skin temperature of 5 K warmer than the surface air temperature was used in computing the moisture-weighting functions in Fig. 2c, where increased sensitivity to moisture can be seen near the surface, particularly in the window channels (bands 29, 31, and 32).

b. Statistical synthetic regression retrieval processing

A computationally efficient method for determining the distribution of atmospheric temperature, moisture, and ozone from satellite sounding measurements uses previously determined statistical relationships between observed or modeled radiances with corresponding atmospheric profiles. In the regression procedure, temperature and moisture are regressed together against radiances from CO_2, water vapor, and window bands. This method is often used to generate a first guess for a physical retrieval algorithm, as is done in the International Television and Infrared Observation Satellite (TIROS) Operational Vertical Sounder (TOVS) Processing Package (ITPP; Smith et al. 1993). The statistical regression algorithm for atmospheric temperature is described in detail in Smith et al. (1970), and is summarized below for cloud-free skies.

The general inverse solution of Eq. (2) for the atmospheric profile can be written as (Smith et al. 1970)

$$\mathbf{X}(i, k) = \mathbf{A}(i, n)\mathbf{Y}(n, k), \tag{5}$$

where i is the number of parameters to be retrieved, k is the number of profiles and surface data in the training

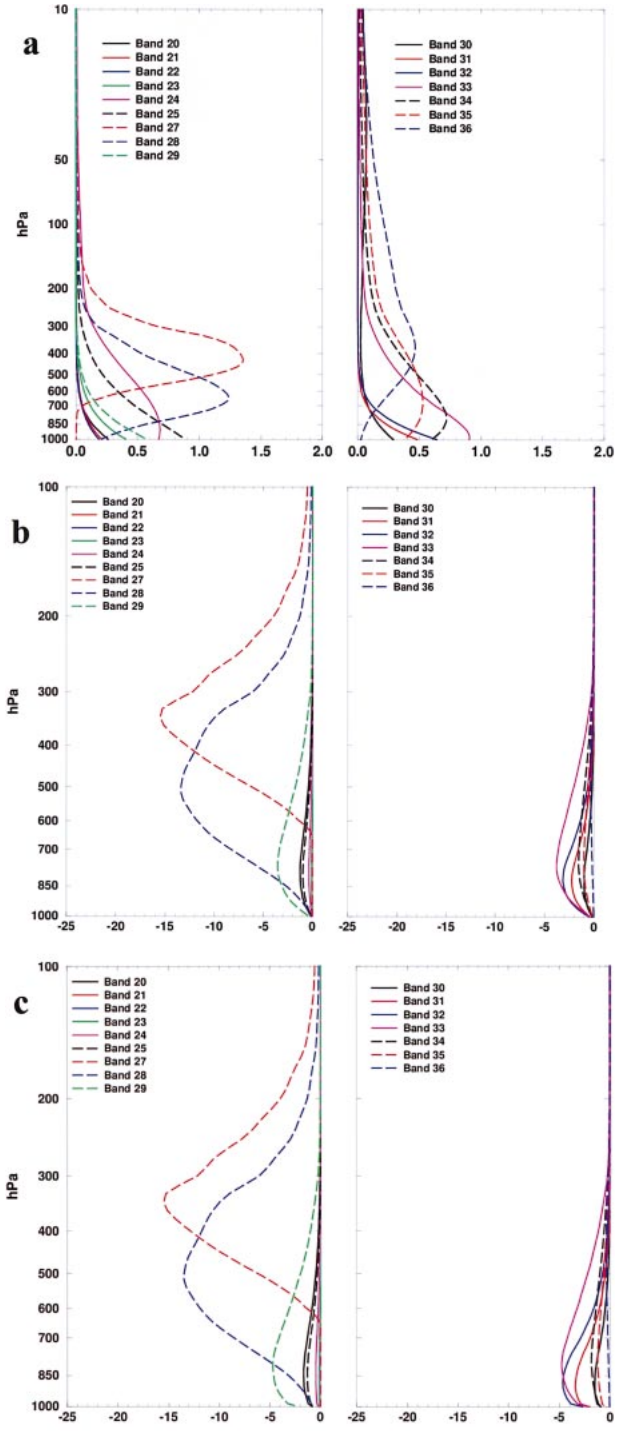

FIG. 2. MODIS-weighting functions based on a *U.S. Standard Atmosphere, 1976* for the MODIS infrared bands 20–25 and 27–36. (a) Temperature-weighting functions are expressed in $[\partial T_b/\partial T(p)]$ and scaled by $d(\ln p)$. (b) Water vapor mixing ratio weighting functions are in $\{\partial T_b/\partial[\ln q(p)]\}$ and scaled by $d(\ln p)$. (c) The water vapor mixing ratio weighting functions as in (b), except with skin temperature 5 K greater than the surface air temperature.

TABLE 2. Predictors and their uncertainty used in the MOD07 regression procedure. BT is brightness temperature and units are specified in the table.

Predictor	Noise used in MOD07 algorithm for *Terra* MODIS	Postlaunch NEΔT averaged over detectors (K)
Band-25–24 BT	0.75 K	0.163 (band 24) 0.086 (band 25)
Band-27 BT	0.75 K	0.376
Band-28 BT	0.75 K	0.193
Band-29 BT	0.189 K	0.189
Band-30 BT	0.75 K	0.241
Band-31 BT	0.167 K	0.167
Band-32 BT	0.192 K	0.192
Band-33 BT	0.75 K	0.308
Band-34 BT	0.75 K	0.379
Band-35 BT	0.75 K	0.366
Band-36 BT	1.05 K	0.586
Surface pressure	5 hPa	—
Percentage of land	0.01%	—
Month	0.1	—
Latitude	0.1°	—

sample, and n is the number of channels and other predictors used in the regression procedure. The statistical regression algorithm seeks a ''best fit'' operator matrix $\mathbf{A}$ that is computed using least squares methods with a large sample of atmospheric temperature and moisture soundings and collocated radiance observations. Minimizing the difference between synthetic observations and the regression model,

$$\frac{\partial}{\partial \mathbf{A}}|\mathbf{AY} - \mathbf{X}|^2 = 0, \tag{6}$$

yields

$$\mathbf{A}(i, n) = \mathbf{X}(i, k)\mathbf{Y}^{\mathrm{T}}(k, n)[\mathbf{Y}(n, k)\mathbf{Y}^{\mathrm{T}}(k, n)]^{-1}, \tag{7}$$

where ($\mathbf{Y}^{\mathrm{T}}$ $\mathbf{Y}$) is the covariance of the radiance observations and ($\mathbf{Y}^{\mathrm{T}}$ $\mathbf{X}$) is the covariance of the radiance observations with the atmospheric profile.

In the MODIS regression procedure, the primary predictors [$\mathbf{Y}$ in Eq. (5)] are infrared spectral band brightness temperatures. The algorithm uses 12 infrared bands with wavelengths between 4.465 and 14.235 μm (see Table 2). Quadratic terms of all brightness temperature predictors are also used as separate predictors to account for the nonlinear relationship of moisture to the MODIS radiances. Surface emissivity effects in the shortwave window bands are mitigated by regressing against band differences [e.g., instead of BT(4.5 μm) and BT(4.4 μm), the difference, BT(4.5 μm) − BT(4.4 μm) is used in the regression, where BT represents brightness temperature]. See section 3d for more discussion on surface emissivity uncertainty. In addition to the primary predictors, estimates of surface pressure, latitude, month, and percentage of land are also used as predictors to improve the retrieval.

Ideally, the radiance predictors $\mathbf{Y}$ would be taken from actual MODIS measurements and used with time- and

space-collocated radiosonde profiles **X** to directly derive the regression coefficients **A**. In such an approach, the regression relationship would not involve any radiative transfer calculations. However, radiosondes are only routinely launched 2 times per day at 0000 and 1200 UTC simultaneously around the earth; *Terra* passes occur at roughly 1100 and 2300 LST each day. It is, therefore, not possible to obtain many time- and space-collocated radiosondes and MODIS radiances that are globally distributed at a wide range of locations. Alternatively, synthetic regression coefficients can be generated from MODIS radiances calculated using a transmittance model with profile input from a global temperature and moisture radiosonde database. The advantage of this approach is that it does not need MODIS radiances collocated in time and space with atmospheric profile data; it requires only historical profile observations. However, it involves the radiative transfer calculations and an accurate forward model in order to obtain a reliable regression relationship. Any uncertainties (e.g., a bias of the forward model) in the radiative calculations will influence the retrieval. To address model uncertainties, radiance bias adjustments have been implemented in the retrieval algorithm, as discussed in section 3b.

In the MODIS retrieval algorithm, the National Oceanic and Atmospheric Administration (NOAA)-88b global dataset of radiosonde observations is used for training the regression. The NOAA-88b dataset was chosen for this purpose to build on previous experience with the sounding algorithm from the Advanced TOVS (ATOVS; Li et al. 2000). See section 3c for more information about the NOAA-88b dataset. Other radiosonde datasets such as the Thermodynamic Initial Guess Retrieval (TIGR)-3 are also being tested for possible operational implementation. The original NOAA-88b data contains 7547 globally distributed clear-sky radiosonde profiles of temperature, moisture, and ozone, along with observations of surface temperature and pressure. Additional radiosonde observations have been added to this dataset for the MODIS retrieval algorithm, as described in section 3c. The radiative transfer calculation of the MODIS spectral band radiances is performed with the PFAAST model for each profile from the training dataset to produce a temperature–moisture–ozone profile–MODIS radiance pair. The synthetic regression coefficients [see Eq. (7)] are generated using the calculated radiances and the matching atmospheric profile. For each training profile, 680 coefficients are generated, corresponding to different local zenith angles from nadir to 65°, with an increment of approximately 0.1°.

The estimated MODIS instrument noise was added to the calculated spectral band radiances before creating the coefficients. The noise was randomly generated with a Gaussian distribution, a standard deviation equal to the NEΔT in Table 2, and an average of zero. The noise used in the algorithm is larger than estimates of postlaunch detector noise to account for variability between the 10 detectors (striping). The correlation in the noise between the spectral bands was not considered in the regression, and it is assumed that any impact of spectral noise correlation on the retrievals should be small. This impact will be further studied in future work.

The predictands, or the parameters to be retrieved by regression, include the temperature profile, logarithm of the water vapor mixing ratio profile, logarithm of the ozone mixing ratio, surface skin temperature, and longwave and shortwave infrared surface emissivities. To perform the retrieval, Eq. (5) is applied to the actual MODIS measurements, where **Y** is now the observed MODIS radiances. Integration of the retrieved profiles yields the total precipitable water (TPW) or total column ozone. Other atmospheric parameters, such as layer temperature and moisture and stability indices, can also be calculated from the predictands. The retrieved water vapor mixing ratio at each pressure level is checked for saturation and the mixing ratio at any level with relative humidity greater than 100% is set equal to the saturation mixing ratio at that level. In addition to integrating retrieved mixing ratio profiles to obtain TPW, TPW is also retrieved directly by integrating the training data profiles and including TPW as a predictand.

To analyze the information contribution from various predictors to the retrieval, a simulation study was performed. In the simulation, 90% of the NOAA-88b profile data samples were used for training, while radiances calculated from the remaining 10% of the profiles were used for testing the retrieval algorithm. The noise added in the simulation is the same as the noise used in the operational algorithm for *Terra* (see Table 2). Figure 3 shows the root-mean-square error (rmse) of the retrieved vertical profiles of temperature and moisture compared with the actual profiles for the 844 independent regression retrievals. The most accurate MODIS temperature retrievals are between 800–400 hPa, where the rmse is approximately 1 K. Near the surface, rmse increases to 2 K. Moisture retrieval accuracy decreases with height from an rmse maximum of 1.5 g kg^{-1} at the lowest levels. The rmse of the ozone profiles reaches a maximum of 0.75 ppmv at the highest levels.

The impact of various predictors on the total precipitable water retrieval was also investigated using retrievals from the simulated data. Figure 4 shows comparisons between actual TPW (integrated from the 844 independent test profiles) and TPW retrieved from radiances calculated from the same profiles. For the simulation results in Fig. 4a, the same NEΔT and predictors were used as in the operational *Terra* MODIS algorithm. Calculating the coefficients without adding artificial noise to the calculated radiances (Fig. 4b) leads to improvement of the rmse from 4.15 mm with added noise to 2.9 mm without. However, for retrievals with true MODIS radiances, it is necessary to add artificial noise to the radiances calculated in the synthetic coefficients to account for striping and other instrument noise. Removing the quadratic terms (individual brightness temperatures

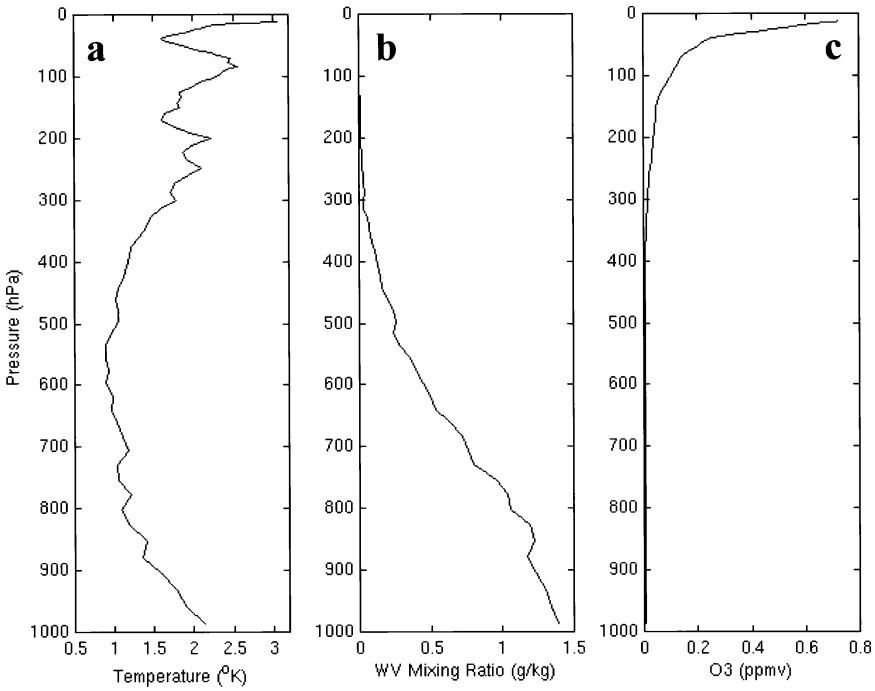

FIG. 3. Rmse of actual compared with retrieved profiles of (a) temperature (K), (b) mixing ratio (g kg^{-1}), and (c) ozone (ppmv). Profiles were taken from an independent sample of 10% of the NOAA-88b data (844 profiles) and retrievals were performed on radiances computed from each profile.

squared) from the predictor list shows an increase in the rmse to 3.2 mm (not shown) from 2.9 mm, computed with no added noise.

c. Nonlinear physical retrieval processing

The statistical regression algorithm has the advantage of computational efficiency, numerical stability, and simplicity. However, it does not account for the physical properties of the radiative transfer equation (RTE). After computing atmospheric profiles from the regression technique, a nonlinear iterative physical algorithm (Li et al. 2000) applied to the RTE often improves the solution. The physical retrieval approach is described in this section.

The physical procedure is based on the regularization method (Li et al. 2000), wherein a penalty function defined by

$$\mathbf{R}(\mathbf{X}^p) = \|\mathbf{R}^m - \mathbf{R}(\mathbf{X}^p)\|^2 + \gamma\|\mathbf{X}^p - \mathbf{X}_0^p\|^2 \quad (8)$$

is minimized to improve the fit of the MODIS spectral band measurements to the regression first guess. In Eq. (8), $\mathbf{X}^p$ is the atmospheric profile to be retrieved, $\mathbf{X}_0^p$ is the initial state of the atmospheric profile or the first guess from regression, $\mathbf{R}^m$ is the vector of the observed MODIS brightness temperatures used in the retrieval process, $\mathbf{R}(\mathbf{X}^p)$ is the vector of calculated MODIS brightness temperatures from an atmospheric state ($\mathbf{X}^p$), and γ is the regularization parameter that can be determined by the discrepancy principle (Li and Huang 1999; Li et al. 2000). The solution provides a balance between MODIS spectral band radiances and the first guess.

A comparison between the regression-based first-guess brightness temperatures and the physical retrieval brightness temperatures is presented in Fig. 5. The results are based on simulated data similar to that detailed in section 2b for Figs. 3 and 4, except that retrievals were performed on only the 394 moist profiles with TPW greater than 17 mm. Only moist cases were used in this comparison because the current physical retrieval algorithm has very little effect on dry cases; the moisture signal is weak in the MODIS IR radiance measurements for a dry atmosphere. The rmse of actual minus retrieved brightness temperature decreased from the regression-based guess to the physical retrieval. The most significant improvement is apparent in the water vapor bands 27 and 28, with the rmse decreasing from 0.8 to 0.2 K for band 27 (6.7 μm), and from 0.6 to 0.2 K for band 28 (7.3 μm). The improvements evident in the brightness temperature calculations using the physical algorithm are also apparent in the retrieved products. For the same 844 simulated radiances as in Fig. 4, the rmse of the actual TPW minus that retrieved using the physical retrieval was 3.6 mm with added noise and 2.5 mm without, compared with 4.15 and 2.9 mm for the regression retrievals with and without noise, respectively.

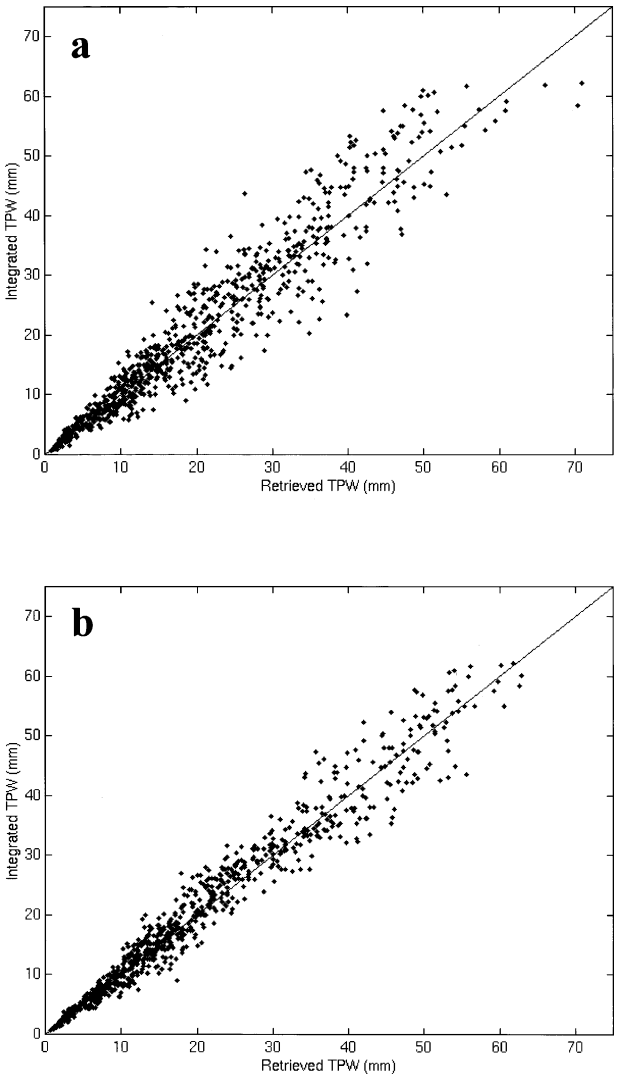

FIG. 4. Comparison of retrieved TPW (mm) with actual TPW from an independent sample of 10% of the NOAA-88b profile data (844 profiles) for the MODIS algorithm (a) with noise added to the radiances calculated for the coefficients and (b) without noise. Rmse for the retrievals with noise is 4.3 mm and it is 2.9 mm without noise. The solid line in each figure shows a 1-to-1 correspondence between retrieved and actual TPW.

In summary, a nonlinear physical retrieval shows some improvement over a synthetic regression retrieval for MODIS retrievals. However, the physical retrieval requires more computation time and, like the synthetic regression used in the MODIS processing, is dependent on the accuracy of the radiative transfer model.

3. Operational implementation

The operational MODIS retrieval algorithm consists of several procedures that include cloud detection, averaging clear radiances from 5 × 5 FOV areas, bias adjustment of MODIS brightness temperatures to account for forward model and instrument errors, synthetic regression retrieval, and an option to perform a physical retrieval. Because of computer limitations, the MODIS MOD07 retrieval algorithm that is operational at the GDAAC processing system includes only the synthetic regression retrieval. A version of the algorithm with the physical retrieval will be available for MODIS direct broadcast processing through IMAPP.

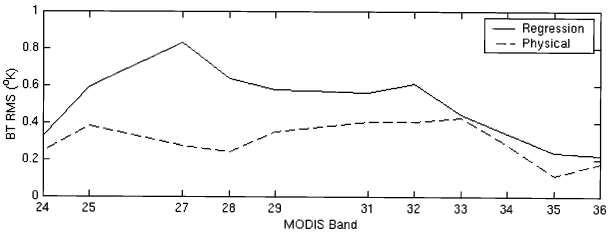

FIG. 5. Rmse (K) for MODIS bands 24, 25, 27–29, and 31–36 of observed minus synthetic regression retrieval brightness temperatures (solid lines) and observed minus physical retrieval brightness temperatures (dashed lines). Brightness temperatures were computed from profile retrievals of the same simulated radiances as in Figs. 3 and 4, except using only moist cases with TPW greater than 17 mm.

a. Cloud detection algorithm

MODIS atmospheric and surface parameter retrievals require clear-sky measurements. The operational MODIS cloud-mask algorithm (Ackerman et al. 1998) is used to identify pixels that are cloud free. The MODIS cloud-mask algorithm determines if a given pixel is clear by combining the results of several spectral threshold tests. A confidence level of clear sky for each pixel is estimated based on a comparison between observed radiances and specified thresholds. The MODIS atmospheric retrieval algorithm requires that at least 5 of the 25 pixels in a 5 × 5 field-of-view area have a 95% or greater confidence of clear by the cloud mask. The retrieval for each 5 × 5 field-of-view area is performed using the average radiance of only those pixels that were considered clear. Experimentation with MODIS retrievals for different requirements for the minimum number of clear pixels showed that requiring that 5 of 25 pixels be clear maximized retrieval coverage, while minimizing undetected cloud contamination. A more strict requirement would further reduce cloud contamination effects but also lead to fewer retrievals. Since the decision to perform a retrieval depends on the validity of the cloud-mask algorithm, cloud contamination may occur if the cloud mask fails to detect a cloud, or the retrieval may not be processed if the cloud-mask falsely identifies a cloud.

b. Radiance bias adjustment in the retrieval processing

The forward model–calculated radiances have biases with respect to the MODIS-measured radiances. There are several possible causes, including calibration errors,

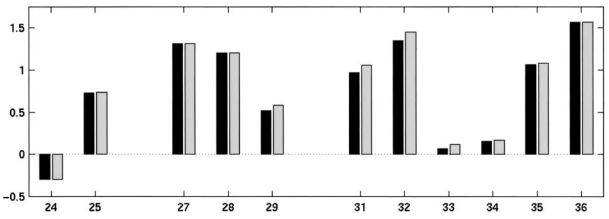

FIG. 6. Average observed minus calculated brightness temperature biases for *Terra* MODIS IR bands 24, 25, 27–29, and 31–36 from 72 clear-sky cases at the SGP ARM CART site from Apr 2001 to Aug 2002. Biases for radiance calculations using skin temperature observed by the IRT (black bars). Synthetic regression-derived skin temperature was used for the calculated radiances in the biases shown as gray bars. No bias is shown for band 30 because of insufficient ozone observations for input to the forward model.

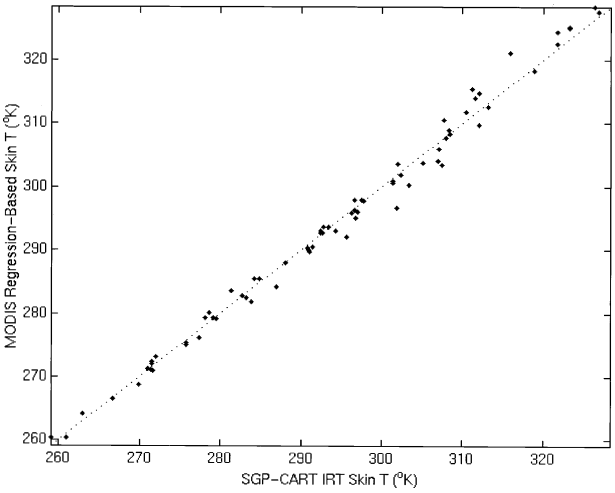

FIG. 7. Comparison of skin temperature (K) computed by MODIS synthetic regression (*y* axis) with that observed by the SGP CART IRT (*x* axis) for the same cases used in Fig. 6. The dotted line shows a 1-to-1 correspondence.

spectral response uncertainty, temperature and moisture profile inaccuracies, and forward model error. The synthetic regression and physical retrieval methods use both measured and calculated radiances and thus require that this bias be minimized. Some of the techniques developed for computing GOES sounder radiance biases with respect to the forward model (Hayden 1988) were adapted to the MODIS atmospheric temperature, moisture, and ozone retrieval algorithm. Bias adjustment for radiative transfer calculation of MODIS spectral band radiances is demonstrated to have a positive impact on the atmospheric product retrievals.

MODIS radiance bias calculations are routinely computed for the Southern Great Plains (SGP) Atmospheric Radiation Measurement (ARM) Cloud and Radiation Test Bed (CART) for clear scenes with MODIS sensor zenith angle less than 35°. Observed MODIS radiances, averaged from a 5×5 field-of-view area, are compared with those computed using the 101-level PFAAST model, with temperature and moisture profile input from National Center for Environmental Prediction (NCEP)'s Global Data Analysis System (GDAS) global analysis data. Skin temperature and emissivity are estimated by regression with MODIS radiances. To establish credibility for the synthetic regression-derived skin temperature input, actual observed skin temperature from the SGP ARM CART ground-based downward-looking infrared thermometer (IRT) measuring the radiating temperature of the ground surface was also used. Figure 6 shows that, on average over 72 clear-sky day and night cases from April 2001 to August 2002, the observed minus calculated radiance biases computed using the regression-based skin temperature differ very little from those computed using the IRT skin temperature. A comparison of the two skin temperatures for the same cases used in computing the biases shows good agreement (Fig. 7); the rmse of the IRT skin temperature compared with MODIS regression-based skin temperature is 1.75 K, and the slope of a linear best fit is 1. Most CART site MODIS radiance biases (expressed as observed minus calculated BT) shown in Fig. 6 are positive, indicating that, on average, the observed MODIS brightness temperatures are warmer than those predicted by the model. Case-to-case variability for each spectral band can be seen in Fig. 8. The high variability in the radiance bias for band 27 is partially due to the significant detector-to-detector differences, or striping, that exists in the radiance data for this band. Some of the variability in this band is also related to differences in the atmospheric moisture; band-27 radiance bias calculations vary as a function of TPW. For this reason, a different band-27 radiance bias correction is applied to moist scenes (TPW $>$ 17 mm) than to dry scenes (TPW $>$ 17 mm).

A comparison of MODIS products at the SGP ARM CART site with and without the radiance bias corrections confirms a significant improvement with the bias corrections. The rmse for TPW sensed by the CART site microwave radiometer (MWR) compared with MODIS TPW for 80 clear-sky cases between April 2001 and October 2002 decreased from 5.9 to 4.1 mm when the bias corrections were applied (not shown). The improvements were primarily apparent for moist cases; the average MWR minus MODIS TPW difference for the 43 cases with TPW greater than 17 mm was 5.6 mm without bias corrections, as compared with 1.24 mm after correction. Because the MODIS retrieval algorithm is applied globally, the biases computed at the SGP ARM CART site are not appropriate for application at other latitudes and for other ecosystem types. Thus, radiance bias corrections have been computed for other regions of the globe; however, they are less well validated.

To compute the global radiance biases, observed MODIS brightness temperatures were compared with calculated brightness temperatures for clear-sky scenes distributed globally with a MODIS-viewing zenith angle $>30°$. Calculations of brightness temperatures were per-

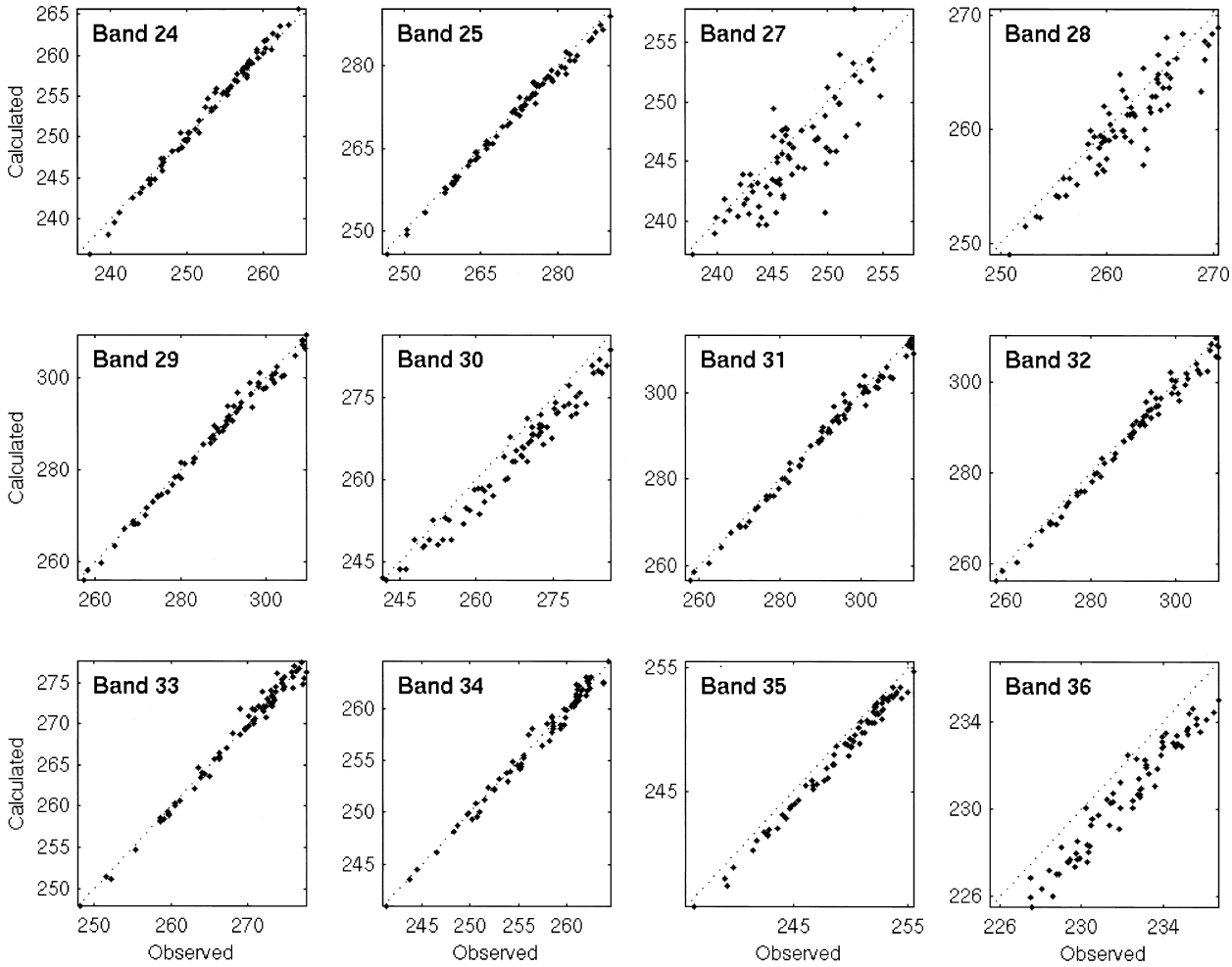

FIG. 8. Calculated vs observed brightness temperatures (K) for each MODIS IR band used in the retrieval algorithm. Each dot represents 1 of the 72 CART cases used in Figs. 6 and 7. The dotted lines show a 1-to-1 correspondence between calculated and observed BT.

formed as outlined above for the SGP CART site with skin temperature and emissivity estimated from regression of MODIS radiances, and temperature and moisture profiles taken from NCEP GDAS analysis. Because there are known difficulties in retrieving skin temperature and emissivity over the desert, these cases were excluded from the global averages. The global radiance biases are separated into six latitudinal zones each for land and ocean. The average global radiance bias calculations for northern midlatitude land agree fairly well with those calculated at the SGP CART site; the rmse of MODIS minus MWR TPW for 80 cases increased only 0.3 mm when using the global radiance bias instead of the SGP CART biases (not shown).

The radiance bias corrections applied in the operational MODIS atmospheric retrieval algorithm will be updated regularly to account for adjustments in the instrument calibration and improvements in the forward model. Future versions of the algorithm will include a more advanced global bias scheme that uses a regression based on predictors that characterize the air mass (e.g., brightness temperatures, surface skin temperature, TPW, and atmospheric layer thickness) similar to that employed on the TOVS (Eyre 1992; Harris and Kelly 2001).

c. Adjustments to the NOAA-88b training dataset

The NOAA-88b dataset contains 7547 globally distributed clear-sky radiosonde observations. Profiles of temperature, moisture, and ozone and surface data from this dataset were used to compute the synthetic regression coefficients for the MODIS statistical retrieval. The temperature and mixing ratio profiles are from radiosondes launched in 1998 at a wide range of locations distributed globally; ozone was derived from solar backscatter ultraviolet (SBUV) collocated profiles. All profiles were extended to 0.005 hPa and interpolated to 101 levels by researchers at NOAA–National Environmental Satellite, Data, and Information Service (NESDIS) who created the dataset.

A surface emissivity and skin temperature were as-

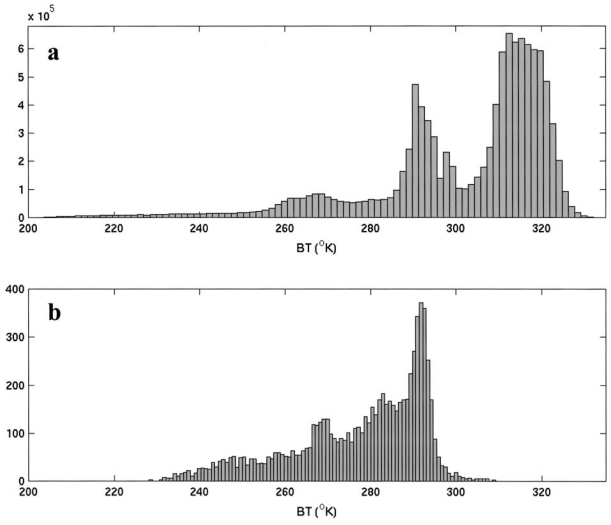

FIG. 9. Histogram of (a) observed MODIS 11-μm brightness temperature from four daytime granules on 2 Jun 2001 (0830, 0835, 1010, and 1150 UTC) over the North African deserts, and (b) computed from a forward model calculation using the original NOAA-88b training profiles and surface data as input. Histogram is expressed in number of profiles for each BT11 (K).

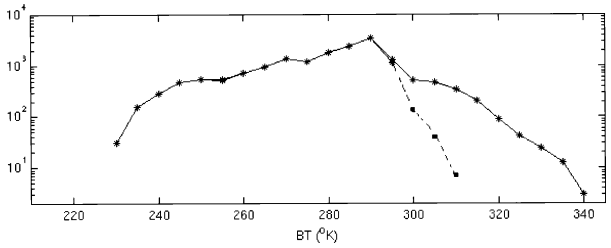

FIG. 10. Frequency of occurrence of 11-μm brightness temperature in the original NOAA-88b training dataset (dashed) and the extended training dataset, including the additional desert radiosondes (solid).

signed to each training profile to be used as input to the forward model because observed surface information is not included in the NOAA-88b profile dataset. The characterization of the surface used in the calculation of the synthetic coefficients is described below. Infrared emissivity spectra were assigned randomly to the training profiles with a Gaussian distribution, standard deviation of 0.05, mean of 0.95 for longwave IR bands (8–13 μm), mean of 0.88 for the 6.7-μm band, and mean of 0.84 for shortwave IR bands (4–5 μm). The difference between the lowest-level radiosonde temperature and the skin temperature to be assigned to the profile was also generated randomly with a Gaussian distribution, but with a mean of 0 K and standard deviation of 10 K. To better represent the range of conditions sensed by MODIS, a second skin temperature was assigned to each training profile in a similar manner. This created a second set of radiance–profile pairs with different skin temperatures, thus, doubling the amount of training data used in the regression. Future work will improve upon this choice of skin temperature and emissivity by employing techniques with more physical bases, including the use of ecosystem-dependent emissivities (Wilber et al. 1999) and deriving physical relationships between surface air and skin temperature.

To limit the retrievals to training data with physical relevance to the observed conditions, the NOAA-88b data were partitioned into seven zones based on the 11-μm brightness temperatures (BT11) calculated from the profiles. The seven zones are BT11 $>$245, 245–269, 269–285, 285–294, 294–300, 300–310, and $>$310 K. Any profiles corresponding to BT11 within 2 K of a zone end point were included in both closest zones. When each retrieval is performed, it uses only that subset of the training data in the same zone as the observed MODIS BT11.

After partitioning, there were insufficient training data in the NOAA-88b dataset for the very warm surfaces (the last two zones, BT11 $>$300 K). Figure 9a shows that many measurements over the North African deserts with BT11 $>$300 K had little to no training data corresponding to a similar BT11 (Fig. 9b). To address this problem, new radiosonde data from the North African desert regions for January–December 2001 were added to the training dataset. Spread equally through the 12 months, 900 radiosonde observations met the criteria of relative humidity $<$90% at each level and physically reasonable behavior; profiles of temperature and moisture from these radiosondes were added to the NOAA-88b dataset. A skin temperature was assigned to the new profiles by adding a positive increment to the temperature of the lowest level in the profile. The increment was derived by taking the absolute value of a random number from a Gaussian distribution with mean of zero and standard deviation of 15 K. These warm skin temperatures were necessary to generate brightness temperatures in the desert region, representative of conditions observed by MODIS, and to add more training in the highest BT11 zones. Figure 10 compares the frequency of occurrence of the 11-μm brightness temperatures for both the original and enhanced NOAA-88b dataset with the extra desert profiles.

Results from a study of retrievals using simulated data (similar to that described in section 2b for Figs. 3 and 4) illustrate the benefit of separating the training data into brightness temperature zones and adding the warm desert profiles. For the 844 independent cases with no noise added to the radiances used in the coefficients, the rmse of retrieved TPW compared with actual TPW decreased to 2.9 mm with BT zones and new profiles (see Fig. 4b) from 4.2 mm without (not shown). The most improvement was evident for moist cases with TPW $>$30 mm.

One example of the improvement in retrievals from MODIS data after partitioning the BT11 into seven zones and adding desert training data is presented in

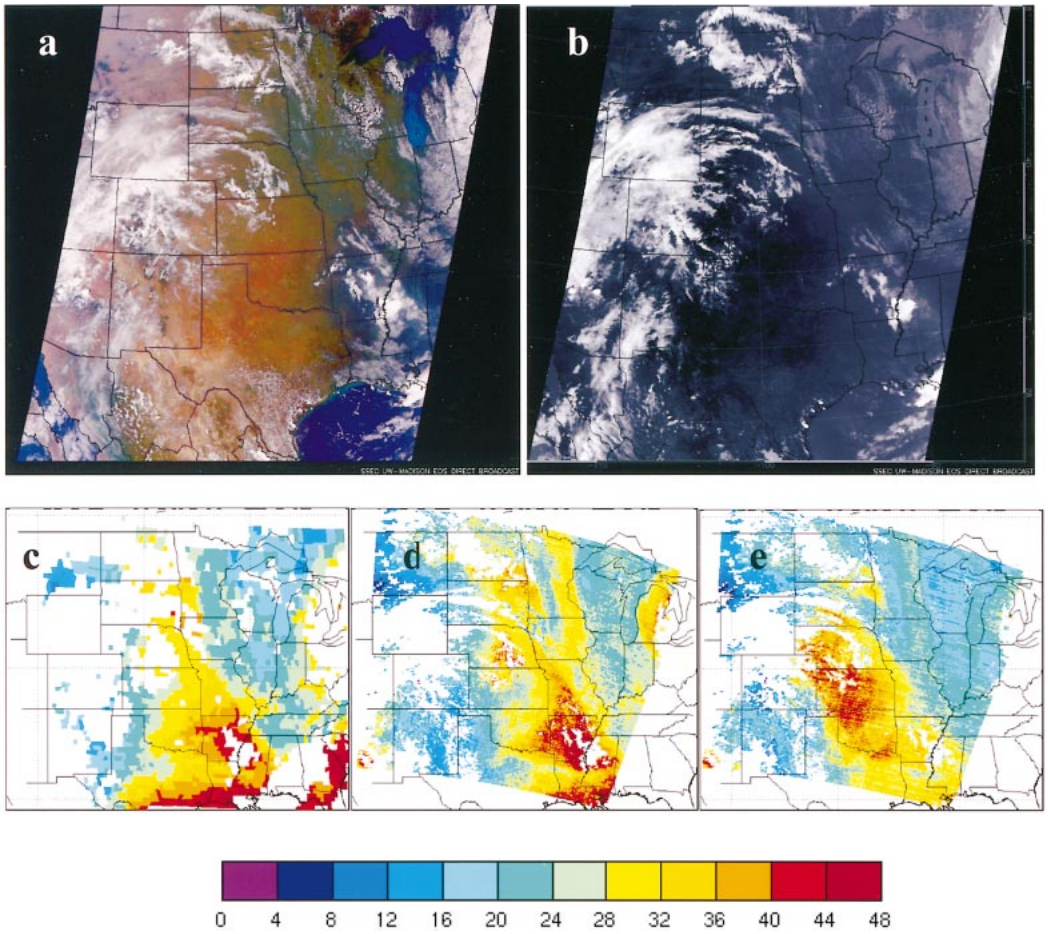

FIG. 11. (top) *Terra* MODIS images from 1735 UTC 20 Aug 2001. (a) True color using MODIS reflectance from bands 1, 4, 3 as red, green, and blue, respectively; (b) MODIS band-31 radiance. Images obtained from University of Wisconsin—Madison's direct broadcast (http://eosdb.ssec.wisc.edu/modisdirect/). (bottom) Comparison of TPW (mm) from the same day retrieved from (c) *GOES-8*, (d) MODIS with the 11-μm BT zones, and (e) MODIS without the 11-μm BT zones. The MODIS granule began at 1735 UTC and the GOES at 1800 UTC.

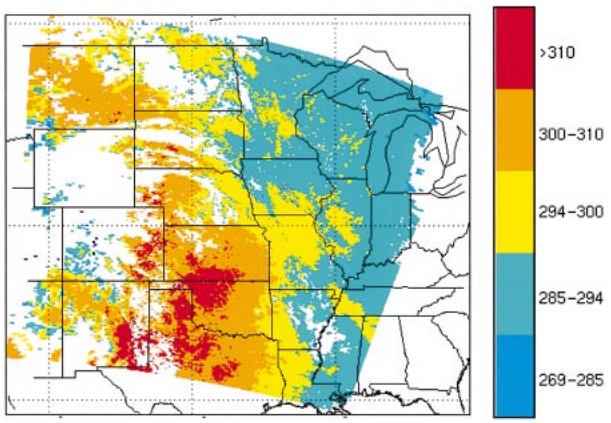

FIG. 12. An 11-μm brightness temperature divided into the same seven zones used in the retrieval algorithm for the same case as shown in Fig. 11. The areas that show the most improvement in the comparison in Fig. 11 are in the warmest two brightness temperature zones.

Fig. 11. True color reflectance and 11-μm radiance images from 20 August 2001 are shown in Figs. 11a and 11b, respectively. A large area of clear sky exists from Texas through Oklahoma and southeastern Kansas. Figures 11c–e compare *GOES-8* TPW with MODIS TPW retrieved with and without the BT zones and new profiles. The MODIS results with the zones and new profiles compare considerably better with the GOES. The area in Kansas and Oklahoma that shows the most improvement has a warm BT11 that falls within the highest two classes (see Fig. 12). This is consistent with results of other cases; the most significant improvements occurred for scenes with BT11 in the two highest classes.

d. Surface emissivity for IR 4.5-μm spectral bands

In most situations the infrared emissivity assigned to the NOAA-88b training dataset accounts for the global variations in emissivity. However, for some regions, such as the deserts of North Africa, the surface emis-

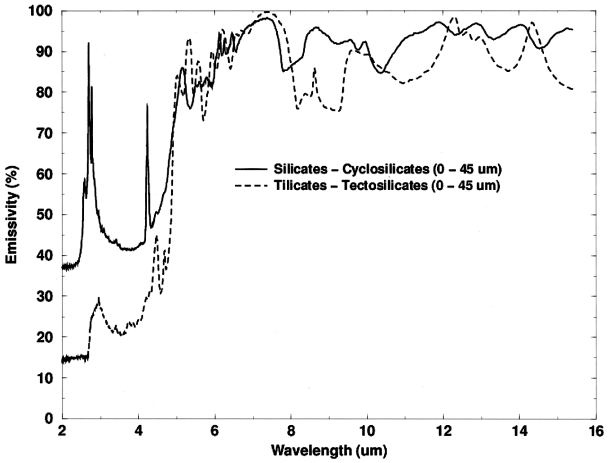

FIG. 13. Measurements of emissivity spectra (%) for two silicates commonly found in desert regions: cyclosilicates (solid line) and tectosilicates (dashed line). Data used in this figure were obtained through the ASTER Spectral Library at the Jet Propulsion Laboratory, California Institute of Technology, Pasadena, CA (available online at http://speclib.jpl.nasa.gov).

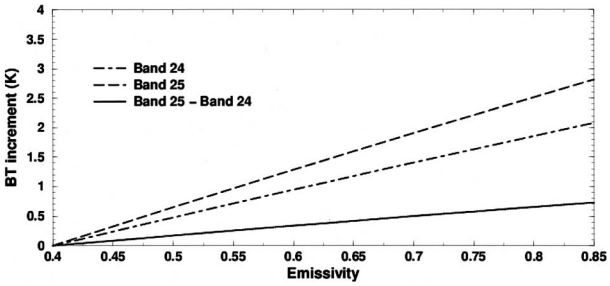

FIG. 14. Difference between the BT calculated at a given emissivity and that calculated with emissivity equal to 0.4 (BT increment; K) for bands 24 and 25 individually (dash–dot and dash, respectively), and for the difference between bands 25 and 24 (solid line). Calculations used a standard U.S. midlatitude summer atmosphere.

sivity has the potential to be significantly lower at 4 than at 11 μm (Salisbury and d'Aria 1992). Figure 13 shows measurements of emissivity spectra from data obtained through the NASA Jet Propulsion Laboratory's spectral library (information available online at http://speclib.jpl.nasa.gov) for two silicates commonly found in desert regions: cyclosilicates and tectosilicates. The emissivity at the 4.5-μm spectral region is extremely low for both minerals, indicating that emissivities in the desert may be as low as 30%–40%. Because emissivities this low are not included in the training dataset, the surface characteristics in the 4.4- and 4.5-μm bands (MODIS bands 24 and 25) were not accurately represented and the MODIS retrievals were excessively moist in the desert regions. To remedy this problem, the difference between these two bands is used as a single predictor instead of using bands 24 and 25 independently; this subtraction removes most of the surface emissivity signal in the regression equation. The BT difference between band 25 and band 24 is found to be much less sensitive to the surface emissivity change than the BT of either of the bands independently. Figure 14 illustrates the advantages of this approach by showing the BT increment, defined as the difference between the BT calculated at a given emissivity and that calculated with emissivity equal to 0.4. The BT increment for the individual bands 24 and 25 is greater than 2.0 K for a surface emissivity of 0.85, while the BT increment for the difference between them is less than 0.8 K. Taking the BT difference between band 25 and band 24 instead of using the bands individually reduces the error in the retrieval due to surface emissivity uncertainties over the desert region. In addition to the surface emissivity effects on 4.5-μm region, there are also effects of nonlocal thermodynamical equilibrium on that region for the radiative transfer modeling. Taking the difference between bands 24 and 25 also minimizes this effect in the retrieval.

4. Evaluation of MOD07 products

Atmospheric retrievals from MODIS have been compared with products from other observing systems at three spatial scales: (a) a fixed point with ground-based measurements at the SGP ARM CART, (b) the continental scale with GOES sounder products, and (c) the global scale with retrievals from the Special Sensor Microwave Imager (SSM/I) and Total Ozone Mapping Spectrometer (TOMS).

a. Comparison of MODIS temperature and moisture with ARM CART observations

Specialized instrumentation at the SGP ARM CART site in Oklahoma facilitates comparisons of MODIS atmospheric products with other observations collocated in time and space. *Terra* passes over the SGP CART daily between 0415 and 0515 UTC and between 1700 and 1800 UTC. Radiosondes are launched 3 times per day at approximately 0530, 1730, and 2330 UTC. Observations of total column moisture are made by the MWR every 40–60 s. An additional comparison is possible with the *GOES-8* sounder (Menzel and Purdom 1994; Menzel et al. 1998) that retrieves TPW hourly.

MODIS retrieved products were compared for 80 clear-sky cases from April 2001 to October 2002. Manual inspection of visible and infrared images excluded any scenes with the possibility of cloud contamination. MODIS sensor zenith angle was less than 50° to the CART site for all cases. To reduce noise due to striping, all retrievals in a 3×3 retrieval area were averaged in this comparison. TPW from MODIS synthetic regression retrievals, the *GOES-8* sounder, radiosondes, and the MWR are compared in Fig. 15. MODIS shows general agreement with the MWR for these cases; however, *GOES-8* sounder and radiosonde observations show better agreement with the MWR. The rmse between MOD-

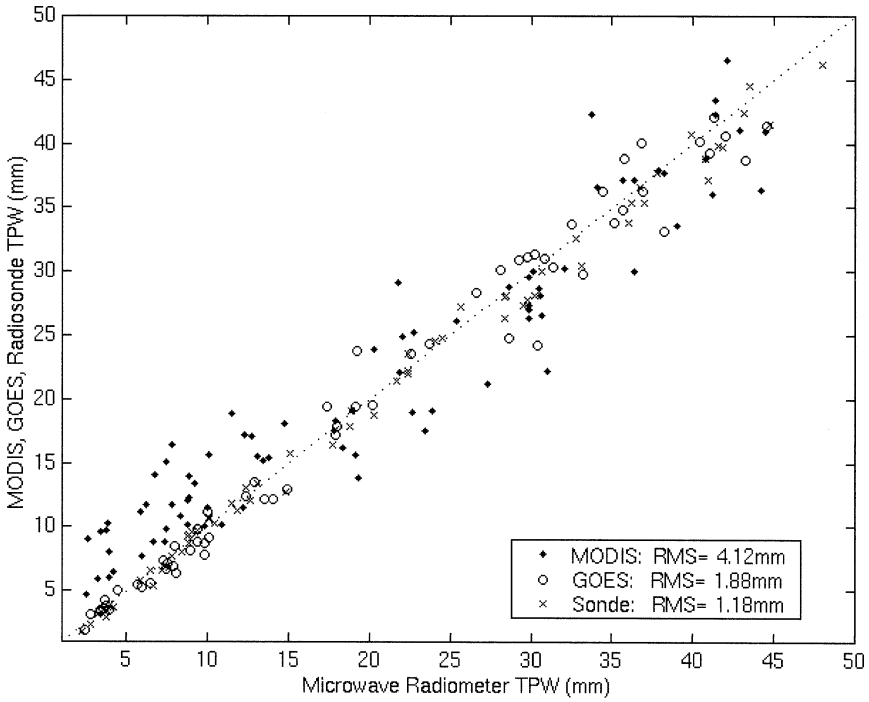

FIG. 15. Comparison of TPW from MODIS synthetic regression (shaded diamond), *GOES-8* (circle), and radiosonde (x) with the SGP ARM CART MWR (mm); 80 cases from Apr 2001 to Oct 2002 are shown in the comparison. The dotted line shows a 1-to-1 correspondence.

IS and MWR TPW collocated in time and space is 4.1 mm for regression retrievals, as compared with 1.9 and 1.2 mm for *GOES-8* and radiosondes, respectively. For the 43 cases with moist atmospheres (TPW $>$ 17 mm), MODIS compares better to the MWR; the rmse between MODIS and MWR TPW is 3.9 mm, as compared with 2.5 mm for GOES and MWR TPW (not shown). On average, for these moist cases, MODIS is 1.2-mm drier than the MWR. For dry atmospheres, MODIS consistently overestimates the total column moisture; MODIS is on average 3.7 mm more moist than the MWR for the 37 dry cases with MWR TPW less than 17 mm. Stephens et al. (1994) observed similar behavior in TOVS total column water vapor and attributed it to a limitation of low spectral resolution infrared sounders in subsidence regions. Use of different band-27 bias corrections for moist and dry cases (see section 3b) improved the retrievals for moist cases but had little effect on the dry cases.

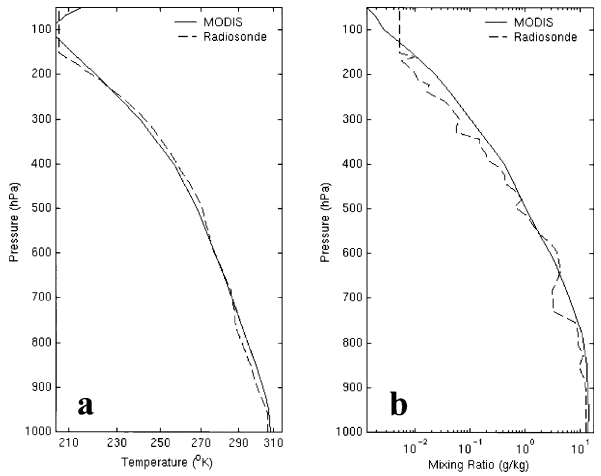

FIG. 16. Comparison of (a) temperature (K) and (b) mixing ratio (g kg^{-1}) on 1 Aug 2001 from the average of nine MODIS profiles in a 3 $\times$ 3 retrieval area surrounding the SGP ARM CART site at 1705 UTC (solid), and a radiosonde launched at 1728 UTC (dashed). In this situation in which the temperature and moisture profiles are smooth, MODIS captures the vertical structure fairly well.

An example comparison of temperature and moisture profiles from a radiosonde at the SGP CART with MODIS regression retrievals of temperature and moisture is shown in Fig. 16. For atmospheres with a fairly monotonic, smooth temperature and moisture distribution, such as that shown here, MODIS retrievals compare well to radiosonde observations. However, in situations with isolated layers of sharply changing temperature or moisture, MODIS is not able to capture the finer-scale structure. Improved sounding capability is expected from the high spectral resolution AIRS on *Aqua* (Susskind et al. 1998).

b. Continental-scale comparisons between MODIS and GOES TPW

On the continental scale, MODIS TPW was compared with *GOES-8* and *GOES-10* sounder retrievals of TPW

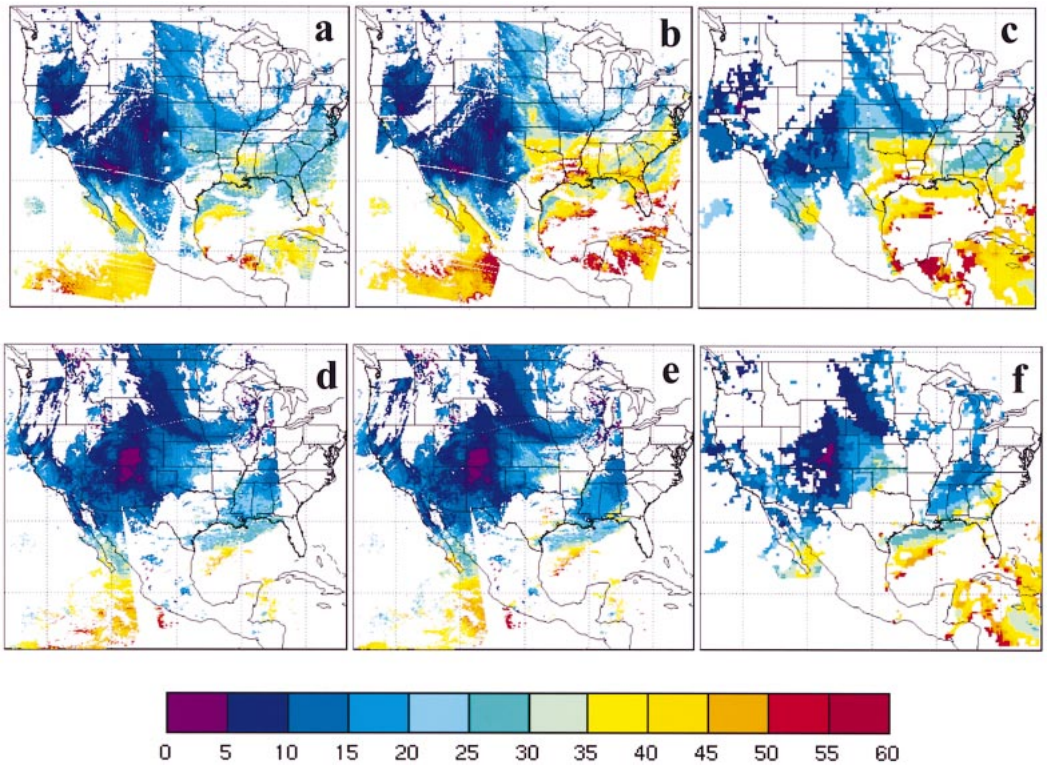

FIG. 17. Total precipitable water (mm) for 2 Jun 2001 over North America retrieved by (a), (d) MODIS synthetic regression (b), (e) MODIS physical, and (c), (f) *GOES-8* and *GOES-10* combined. (top) (a)–(c) Daytime retrievals (four MODIS granules from 1640–1830 UTC; GOES at 1800 UTC) and (bottom) (d)–(f) nighttime retrievals (five MODIS granules from 0435–0625 UTC; GOES at 0600 UTC). The slight discontinuity visible in Oklahoma in the MODIS daytime retrievals occurs where granules from the two subsequent overpasses, separated by 1 h and 40 min, intersect.

over the continental United States and Mexico. GOES TPW has been well validated (Schmit et al. 2002) and has a resolution at the subsatellite point of 10 km. GOES uses radiances measured from a 3 × 3 field-of-view area (approximately 30-km resolution) to retrieve one atmospheric profile, while MODIS has nadir resolution of 1 km and uses a 5 × 5 field-of-view area (5-km resolution). Unlike the MODIS retrieval, GOES hourly radiance measurements are supplemented with hourly surface observations of temperature and moisture as additional information in the GOES retrieval. MODIS and GOES retrieval procedures also use different first-guess profiles; GOES uses a numerical model forecast, while MODIS uses the previously described synthetic regression retrieval.

Figure 17 compares MODIS TPW with TPW retrieved by the *GOES-8* and *GOES-10* sounders over North America for 2 June 2001 during the day and at night. MODIS and GOES show fairly good agreement except the daytime MODIS TPW retrieved by regression is drier than GOES over Oklahoma, Arkansas, and the Gulf of Mexico. TPW retrieved by physical retrieval shows better agreement with GOES in these areas.

c. Global comparisons of MODIS products with SSMI and TOMS

Global TPW from MODIS atmospheric retrievals is compared with TPW from the Defense Meteorological Satellite Program (DMSP) SSM/I (Alishouse 1990; Ferraro et al. 1996; Wentz 1997) for 22 May 2002 in Fig. 18. The SSM/I (resolution 12.5 km) TPW retrievals for clear or cloudy skies over ocean use the 22- and 37-GHz microwave channels. MODIS and SSM/I show similar patterns of TPW distribution and similar magnitudes, however, MODIS retrievals are somewhat less moist over tropical oceans. Some of the differences can be attributed to MODIS TPW retrievals occurring only in clear pixels and, thus, not capturing the moist environment associated with clouds. Other differences may be attributed to the time differences between the two satellite overpasses.

In order to predict the evolution of ozone on timescales of a few days to 1 week, reliable measurements of ozone distribution are needed. The NASA Goddard Space Flight Center (GSFC) TOMS instrument (Bowman and Krueger 1985; McPeters et al. 1998) onboard the Earth Probe (EP) satellite measures backscattered

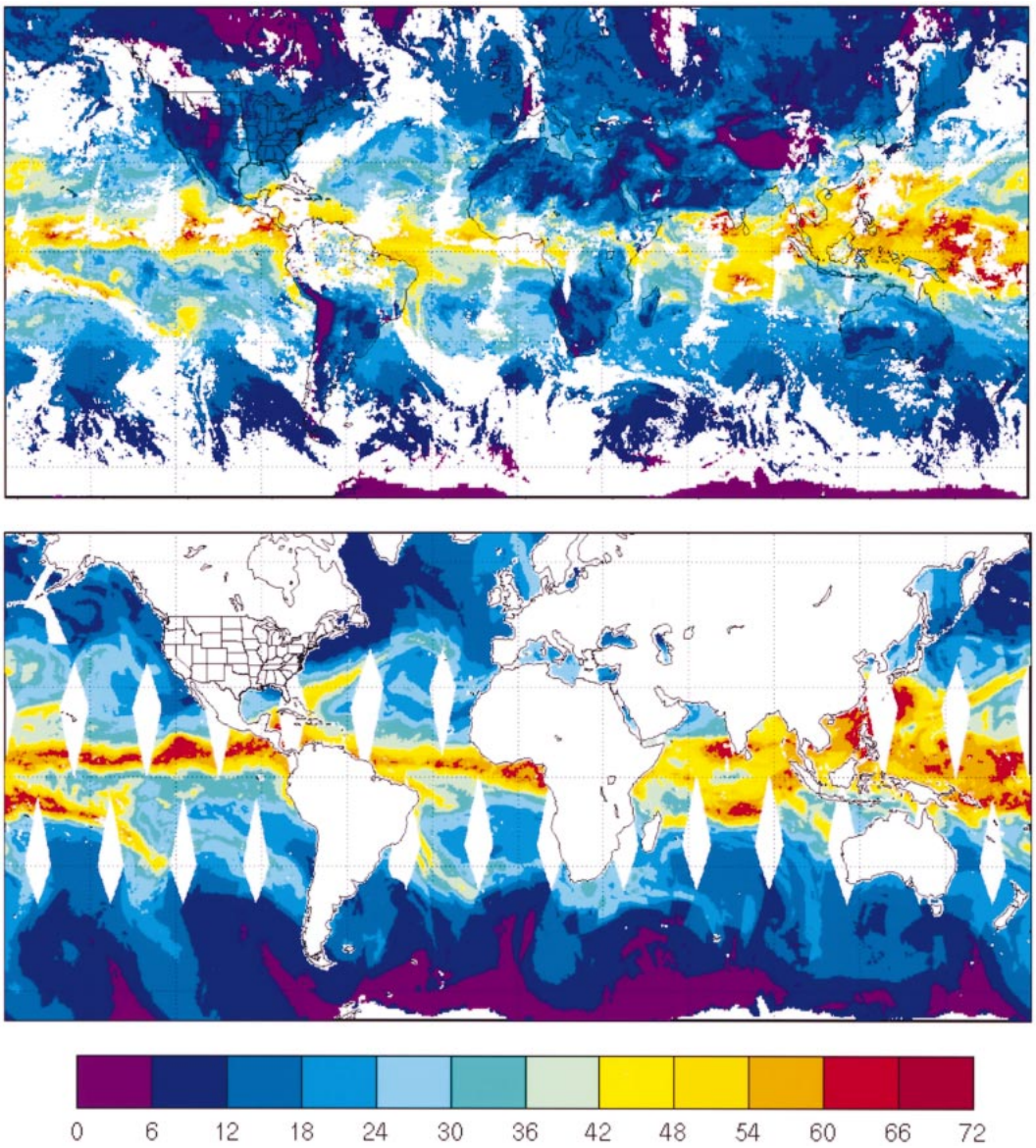

FIG. 18. (top) MODIS TPW (mm) and (bottom) SSM/I TPW (mm) from the *F-14* satellite on 22 May 2002. Retrievals from ascending and descending passes were averaged to obtain these values. The color scale is the same for both MODIS and SSM/I and is shown below the two images. SSM/I data were obtained through the Remote Sensing Systems SSM/I Web page at http://www.ssmi.com. MODIS data were degraded to 25-km resolution from the original 5-km resolution in this figure. White areas in the MODIS image are areas where no retrievals were performed because of the presence of clouds. SSM/I retrievals are performed for both clear and cloudy skies, but they are not performed over land.

ultraviolet solar radiation and cannot provide measurements at night. High-spatial-resolution IR radiance measurements at 9.6 μm (band 30) from MODIS allow ozone estimates during both day and night.

MODIS total column ozone retrievals are compared with TOMS ozone from 22 May 2002 in Fig. 19. The general distribution of ozone from TOMS is similar to that from MODIS. A quantitative comparison for the same day between TOMS and MODIS ozone (Fig. 20) shows percent errors of less than 10% for latitudes between $\pm 20°$. Errors increase toward the Poles, with the highest errors at the South Pole, where very few training data exist.

5. Discussion

Retrieval accuracy, computation efficiency, and retrieval validation are important considerations when applying the operational algorithm to real-time MODIS data processing. The accuracy of the retrievals depends

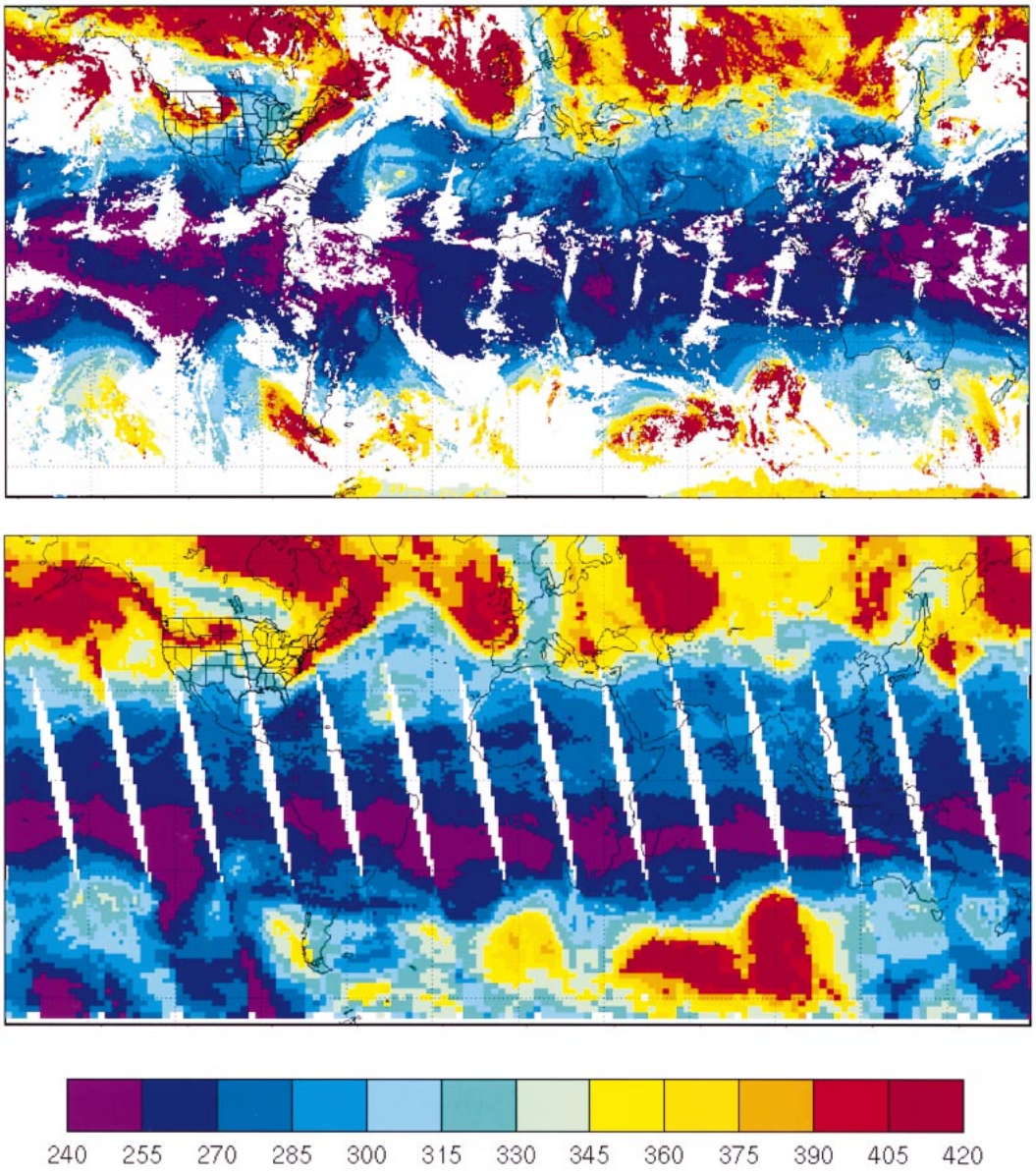

FIG. 19. Total column ozone (Dobson units) for 22 May 2002 for (top) MODIS and (bottom) TOMS. TOMS data were obtained from the NASA GSFC TOMS Web page at http://toms.gsfc.nasa.gov/ozone/ozone.html. The color scale is the same for both MODIS and TOMS and is shown below the two images.

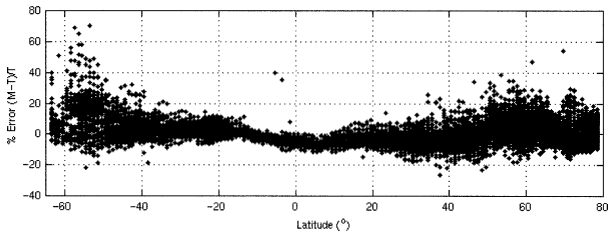

FIG. 20. Percent error for MODIS ozone retrievals in comparison with TOMS ozone as a function of latitude for the same day as shown in Fig. 19.

on the instrument calibration, navigation, and coregistration in the infrared bands; the MODIS is assumed to be calibrated within the instrument noise, navigated within one FOV, and coregistered within two-tenths of a FOV. Several sources of errors must be addressed. First, forward model errors can influence the retrievals. These may be due to atmospheric transmittance calculation error because the transmittance is computed by a fast regression procedure rather than by an accurate line-by-line model; they may be due to inaccurate or insufficient representation of the atmospheric temperature and moisture profiles in the training dataset; or they may be due to the surface uncertainties, such as surface el-

evation, emissivity, and skin temperature. Improvement of the forward model is important for deriving the MODIS products with a high level of accuracy.

In addition, the MODIS instrument detector noise and calibration error (observation error) can have an impact on the retrieval accuracy. Large observation errors result in poor MODIS atmospheric products. Detector-to-detector differences in the spectral response functions within a band have been shown to produce 0.5%–1.0% differences in radiance measurements in the IR thermal bands. This is seen as detector striping (called banding by some investigators) within a scene. Well-calibrated radiance measurements without (or with reduced) striping noise are expected to improve the quality of the MODIS atmospheric products presented in this paper. Cloud detection errors may also have a negative impact on the retrieval products. Regions with cloud contamination in the MODIS retrievals show inaccurate moisture and temperature.

Computation efficiency realized by regression methods enables fast retrieval of atmospheric products. The physical retrieval takes more computation time, therefore, it is not possible to apply both the regression and physical retrieval procedures to process global MODIS data operationally at the Distributed Active Archive Center (DAAC). Regional MODIS data received in near–real time by direct broadcast MODIS stations can be processed using both algorithms.

An advantage of MODIS over lower spatial resolution infrared sounders is that it can provide good retrieval coverage under broken cloud conditions and, thus, delineate the horizontal gradients of moisture distribution. To illustrate the value of higher resolution, Fig. 21 compares MODIS TPW retrievals from the *Aqua* satellite with full 1-km resolution to retrievals averaged up to 10-km spatial resolution. The reduced-spatial-resolution retrievals degrade the gradients resolved at 1 km and reduce some of the product coverage. Full-resolution MODIS 1-km retrievals are important for studying the future operational sounder and image systems, such as the planned geostationary Hyperspectral Environmental Suite (HES) and Advanced Baseline Imager (ABI).

A challenge is to maintain adequate global training data so that the synthetic regression algorithm produces accurate atmospheric retrievals. A further challenge is to accommodate special regions, such as the Sahara, where the surface characteristics are unique (very warm and dry, and the surface IR emissivity is lower than in other regions). The operational MODIS algorithm is still evolving in order to meet these challenges.

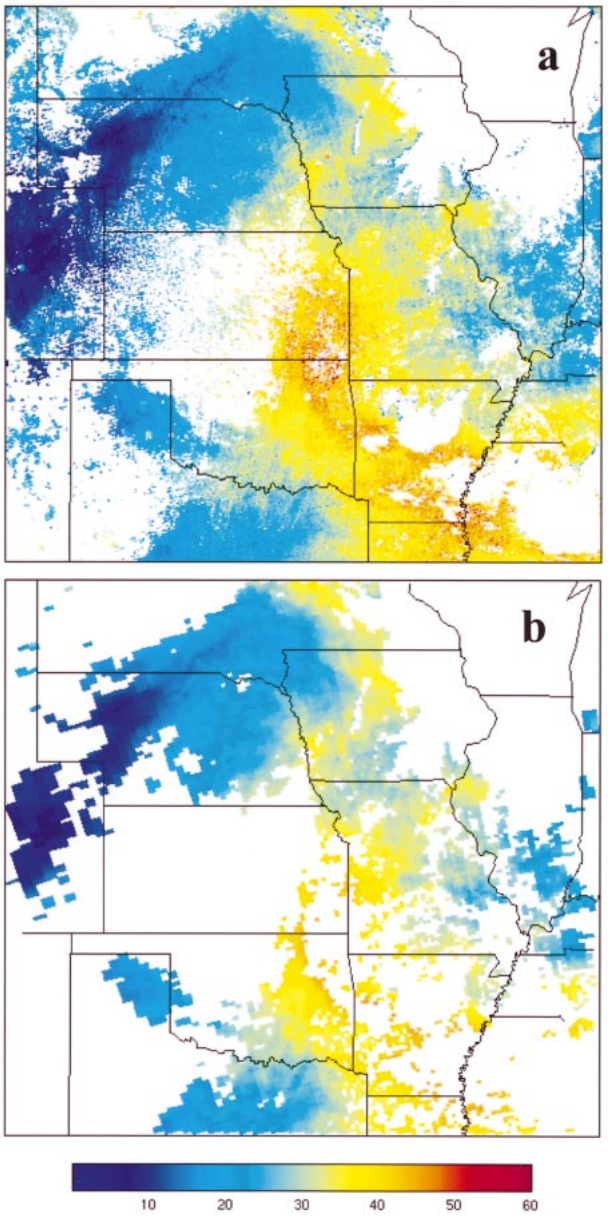

FIG. 21. *Aqua* MODIS TPW (mm) from 20 Jul 2002 with (a) 1-km retrievals and (b) averaged up to 10 km; 10-km retrievals were performed when at least 80% of the pixels are clear.

6. Conclusions and future work

This paper describes the operational atmospheric retrieval algorithms for global DAAC and direct broadcast MODIS data processing. Issues regarding training profiles, noise performance, forward model bias, and low surface emissivity over desert regions are addressed. Comparison of MODIS TPW with ground-based instrumentation at the SGP ARM CART site reveals that MODIS agrees with the MWR, with an rmse of 4.1 mm. For moist scenes with TPW greater than 17 mm, MODIS is on average 1.2 mm drier than the MWR, with an rmse of 3.9 mm; for dry scenes, MODIS is on average 3.7 mm more moist than the MWR. The physical retrievals show improvement of 0.8 mm in rmse over the synthetic regression retrievals for moist cases. More comparisons with ground-based instrumentation are planned; these will include other ARM CART sites in the tropical western Pacific and in Barrow, Alaska. On large scales,

MODIS products show good agreement in spatial distribution when compared with GOES, SSM/I and TOMS.

The atmospheric MOD07 algorithm performs retrievals of atmospheric temperature and moisture layers, total precipitable water, and total column ozone. While MODIS is not per se a sounding instrument, the information content of the high-spatial-resolution infrared multispectral radiance observations can improve upon a priori definitions of atmospheric state by providing better delineation of horizontal gradients.

Future work to improve the algorithm will include enhancing the training database with more radiosonde observations, particularly in under-represented polar areas. In addition, use of new training datasets, such as TIGR-3, in the synthetic regression will be tested. Surface emissivity based on ecosystem type will be investigated to improve the characterization of the surface in the training data. A more physical basis for assigning a skin temperature to each training profile will also be investigated. Improvements to the radiance bias corrections are planned, including adding a seasonal variation to the global radiance bias values, accounting for small-scale variations in bias, and developing a regression relationship between the radiance bias and measured radiances. Mitigation of the relatively high level of noise due to nonuniform detector-to-detector response (striping) will be investigated.

Terra MODIS algorithms have been adapted to the second MODIS instrument onboard the *Aqua* platform. The new platform will double the frequency of global coverage and allow for more consistent monitoring of temperature, moisture, and ozone. Early results from *Aqua* MODIS show considerable reduction in striping. The smoother fields retrieved from *Aqua* MODIS provide better depiction of gradients and allow full use of the high spatial resolution measurements. Future work will focus on validation and applications of the *Aqua* MODIS temperature, moisture, surface temperature, and ozone retrievals. In addition, retrievals based on a combination of MODIS and AIRS radiances from *Aqua* will be investigated to take advantage of the high spectral resolution (hence, high vertical spatial resolution) of AIRS and the high horizontal spatial resolution of MODIS.

Acknowledgments. The authors thank the MODIS group at the University of Wisconsin—Madison CIMSS for their assistance in this work, including Chris Moeller for help with instrument calibration and noise estimates; Kathy Strabala for applying the MOD07 algorithm into the IMAPP software; Richard Frey, Steve Ackerman, and Hong Zhang for assistance with the cloud mask; and Bryan Baum (NASA/LaRC) for useful discussions. Tim Schmit of NOAA/NESDIS helped with the comparisons with GOES sounder retrievals. A note of thanks goes to Hal Woolf of CIMSS who provided the MODIS fast radiative transfer model. Rich Hucek of the MODIS Science Data Support Team assisted with implementing the operational MOD07 algorithm at the GSFC DAAC. We gratefully acknowledge the helpful comments by three anonymous reviewers. ARM CART site data used in this work were obtained from the Atmospheric Radiation Measurement Program sponsored by the U.S. Department of Energy, Office of Science, Office of Biological and Environmental Research, Environmental Sciences Division. Measurements of emissivity spectra were obtained through the ASTER Spectral Library at the Jet Propulsion Laboratory, California Institute of Technology, Pasadena, California. SSM/I TPW data were obtained from Remote Sensing Systems. TOMS data were obtained through NASA GSFC. This work was funded by NASA through NAS5-31367 and NAG5-9389.

REFERENCES

Ackerman, S. A., K. I. Strabala, W. P. Menzel, R. A. Frey, C. C. Moeller, and L. E. Gumley, 1998: Discriminating clear sky from clouds with MODIS. *J. Geophys. Res.,* **103,** 32 141–32 157.

Alishouse, J. C., S. Snyder, J. Vongsathorn, and R. R. Ferraro, 1990: Determination of oceanic total precipitable water from the SSM/I. *IEEE Trans. Geosci. Remote Sens.,* **28,** 811–816.

Bowman, K. P., and A. J. Krueger, 1985: A global climatology of total ozone from the *Nimbus-7* Total Ozone Mapping Spectrometer. *J. Geophys. Res.,* **90,** 7967–7976.

Eyre, J. R., 1992: A bias correction scheme for simulated TOVS brightness temperatures. ECMWF Tech. Memo. 186, 28 pp.

——, and H. M. Woolf, 1988: Transmittance of atmospheric gases in the microwave region: A fast model. *Appl. Opt.,* **25,** 3244–3249.

Ferraro, R. R., N. C. Grody, F. Weng, and A. Basist, 1996: An eight-year (1987–1994) time series of rainfall, clouds, water vapor, snow cover, and sea ice derived from SSM/I measurements. *Bull. Amer. Meteor. Soc.,* **77,** 891–906.

Frey, R. A., B. A. Baum, W. P. Menzel, S. A. Ackerman, C. C. Moeller, and J. D. Spinhirne, 1999: A comparison of cloud top heights computed from airborne lidar and MAS radiance data using CO_2 slicing. *J. Geophys. Res.,* **104,** 24 547–24 555.

Hannon, S., L. L. Strow, and W. W. McMillan, 1996: Atmospheric infrared fast transmittance models: A comparison of two approaches. *Proc. Conf. on Optical Spectroscopic Techniques and Instrumentation for Atmospheric and Space Research II,* Denver, CO, SPIE, 94–105.

Harris, B. A., and G. Kelly, 2001: A satellite radiance bias correction scheme for radiance assimilation. *Quart. J. Roy. Meteor. Soc.,* **127,** 1453–1468.

Hayden, C. M., 1988: GOES-VAS simultaneous temperature-moisture retrieval algorithm. *J. Appl. Meteor.,* **27,** 705–733.

King, M. D., Y. J. Kaufman, W. P. Menzel, and D. Tanré, 1992: Remote sensing of cloud, aerosol, and water vapor properties from the Moderate Resolution Imaging Spectrometer (MODIS). *IEEE Trans. Geosci. Remote Sens.,* **30,** 2–27.

Li, J., 1994: Temperature and water vapor weighting functions from radiative transfer equation with surface emissivity and solar reflectivity. *Adv. Atmos. Sci.,* **11,** 421–426.

——, and H.-L. Huang, 1999: Retrieval of atmospheric profiles from satellite sounder measurements by use of the discrepancy principle. *Appl. Optics,* **38,** 916–923.

——, W. Wolf, W. P. Menzel, W. Zhang, H.-L. Huang, and T. H. Achtor, 2000: Global soundings of the atmosphere from ATOVS measurements: The algorithm and validation. *J. Appl. Meteor.,* **39,** 1248–1268.

——, C. C. Schmidt, J. P. Nelson, T. J. Schmit, and W. P. Menzel,

2001: Estimation of total ozone from GOES sounder radiances with high temporal resolution. *J. Atmos. Oceanic Technol.*, **18,** 157–168.

McPeters, R. D., and Coauthors, 1998: Earth Probe Total Ozone Mapping Spectrometer (TOMS) data products user's guide. NASA Reference Publ. 1998-206895, 64 pp. [Available from NASA Center for AeroSpace Information, 800 Elkridge Landing Rd., Linthicum Heights, MD 21090.]

Menzel, W. P., and J. F. W. Purdom, 1994: Introducing GOES-I: The first of a new generation of geostationary operational environmental satellites. *Bull. Amer. Meteor. Soc.*, **75,** 757–781.

——, F. C. Holt, T. J. Schmit, R. M. Aune, A. J. Schreiner, G. S. Wade, and D. G. Gray, 1998: Application of *GOES-8/9* soundings to weather forecasting and nowcasting. *Bull. Amer. Meteor. Soc.*, **79,** 2059–2078.

Rothman, L. S., and Coauthors, 1998: The HITRAN molecular spectroscopic database and HAWKS (HITRAN Atmospheric Workstation). *J. Quant. Spectrosc. Radiat. Transfer*, **60,** 665–710.

Salisbury, J. W., and D. M. d'Aria, 1992: Emissivity of terrestrial materials in the 8–14 mm atmospheric window. *Remote Sens Environ.*, **42,** 83–106.

Schmit, T. J., W. F. Feltz, W. P. Menzel, J. Jung, A. P. Noel, J. N. Heil, J. P. Nelson, and G. S. Wade, 2002: Validation and use of GOES sounder moisture information. *Wea. Forecasting*, **17,** 139–154.

Smith, W. L., H. M. Woolf, and W. J. Jacob, 1970: A regression method for obtaining real-time temperature and geopotential height profiles from satellite spectrometer measurements and its application to *Nimbus 3* "SIRS" observations. *Mon. Wea. Rev.*, **98,** 582–603.

——, H. M. Woolf, S. J. Nieman, and T. H. Achtor, 1993: ITPP-5—The use of AVHRR and TIGR in TOVS data processing. *Proc. Seventh Int. TOVS Study Conf.*, Igls, Austria, International Radiation Commission, 443–453.

Stephens, G. L., D. L. Jackson, and J. J. Bates, 1994: A comparison of SSM/I and TOVS column water vapor data over the global oceans. *Meteor. Atmos. Phys.*, **54,** 183–201.

Susskind, J., C. Barnet, and J. Blaisdell, 1998: Determination of atmospheric and surface parameters from simulated AIRS/AMSU/HSB sounding data: Retrieval and cloud clearing methodology. *Adv. Space Res.*, **21,** 369–384.

Wentz, F. J., 1997: A well-calibrated ocean algorithm for SSM/I. *J. Geophys. Res.*, **102,** 8703–8718.

Wilber, A. C., D. P. Kratz, and S. K. Gupta, 1999: Surface emissivity maps for use in satellite retrievals of longwave radiation. NASA Tech. Publ. NASA/TP-1999-209362, 35 pp. [Available online at http://techreports.larc.nasa.gov/ltrs/.]